

Model-Independent Determination of the Spin of the Ω^- and Its Polarization Alignment in $\psi(3686) \rightarrow \Omega^- \bar{\Omega}^+$

M. Ablikim,¹ M. N. Achasov,^{10,c} P. Adlarson,⁶⁴ S. Ahmed,¹⁵ M. Albrecht,⁴ A. Amoroso,^{63a,63c} Q. An,^{60,48} Anita,²¹ Y. Bai,⁴⁷ O. Bakina,²⁹ R. Baldini Ferroli,^{23a} I. Balossino,^{24a} Y. Ban,^{38,k} K. Begzsuren,²⁶ J. V. Bennett,⁵ N. Berger,²⁸ M. Bertani,^{23a} D. Bettoni,^{24a} F. Bianchi,^{63a,63c} J. Biernat,⁶⁴ J. Bloms,⁵⁷ A. Bortone,^{63a,63c} I. Boyko,²⁹ R. A. Briere,⁵ H. Cai,⁶⁵ X. Cai,^{1,48} A. Calcaterra,^{23a} G. F. Cao,^{1,52} N. Cao,^{1,52} S. A. Cetin,^{51b} J. F. Chang,^{1,48} W. L. Chang,^{1,52} G. Chelkov,^{29,b} D. Y. Chen,⁶ G. Chen,¹ H. S. Chen,^{1,52} M. L. Chen,^{1,48} S. J. Chen,³⁶ X. R. Chen,²⁵ Y. B. Chen,^{1,48} W. S. Cheng,^{63c} G. Cibinetto,^{24a} F. Cossio,^{63c} X. F. Cui,³⁷ H. L. Dai,^{1,48} J. P. Dai,^{42,g} X. C. Dai,^{1,52} A. Dbeyssi,¹⁵ R. B. de Boer,⁴ D. Dedovich,²⁹ Z. Y. Deng,¹ A. Denig,²⁸ I. Denysenko,²⁹ M. Destefanis,^{63a,63c} F. De Mori,^{63a,63c} Y. Ding,³⁴ C. Dong,³⁷ J. Dong,^{1,48} L. Y. Dong,^{1,52} M. Y. Dong,^{1,48,52} S. X. Du,⁶⁸ J. Fang,^{1,48} S. S. Fang,^{1,52} Y. Fang,¹ R. Farinelli,^{24a} L. Fava,^{63b,63c} F. Feldbauer,⁴ G. Felici,^{23a} C. Q. Feng,^{60,48} M. Fritsch,⁴ C. D. Fu,¹ Y. Fu,¹ X. L. Gao,^{60,48} Y. Gao,⁶¹ Y. Gao,^{38,k} Y. G. Gao,⁶ I. Garzia,^{24a,24b} E. M. Gersabeck,⁵⁵ A. Gilman,⁵⁶ K. Goetzen,¹¹ L. Gong,³⁷ W. X. Gong,^{1,48} W. Gradl,²⁸ M. Greco,^{63a,63c} L. M. Gu,³⁶ M. H. Gu,^{1,48} S. Gu,² Y. T. Gu,¹³ C. Y. Guan,^{1,52} A. Q. Guo,²² L. B. Guo,³⁵ R. P. Guo,⁴⁰ Y. P. Guo,²⁸ Y. P. Guo,^{9,h} A. Guskov,²⁹ S. Han,⁶⁵ T. T. Han,⁴¹ T. Z. Han,^{9,h} X. Q. Hao,¹⁶ F. A. Harris,⁵³ K. L. He,^{1,52} F. H. Heinsius,⁴ T. Held,⁴ Y. K. Heng,^{1,48,52} M. Himmelreich,^{11,f} T. Holtmann,⁴ Y. R. Hou,⁵² Z. L. Hou,¹ H. M. Hu,^{1,52} J. F. Hu,^{42,g} T. Hu,^{1,48,52} Y. Hu,¹ G. S. Huang,^{60,48} L. Q. Huang,⁶¹ X. T. Huang,⁴¹ Z. Huang,^{38,k} N. Huesken,⁵⁷ T. Hussain,⁶² W. Ikegami Andersson,⁶⁴ W. Imoehl,²² M. Irshad,^{60,48} S. Jaeger,⁴ S. Janchiv,^{26,j} Q. Ji,¹ Q. P. Ji,¹⁶ X. B. Ji,^{1,52} X. L. Ji,^{1,48} H. B. Jiang,⁴¹ X. S. Jiang,^{1,48,52} X. Y. Jiang,³⁷ J. B. Jiao,⁴¹ Z. Jiao,¹⁸ S. Jin,³⁶ Y. Jin,⁵⁴ T. Johansson,⁶⁴ N. Kalantar-Nayestanaki,³¹ X. S. Kang,³⁴ R. Kappert,³¹ M. Kavatsyuk,³¹ B. C. Ke,^{43,1} I. K. Keshk,⁴ A. Khoukaz,⁵⁷ P. Kiese,²⁸ R. Kiuchi,¹ R. Kliemt,¹¹ L. Koch,³⁰ O. B. Kolcu,^{51b,e} B. Kopf,⁴ M. Kuemmel,⁴ M. Kuessner,⁴ A. Kupsc,⁶⁴ M. G. Kurth,^{1,52} W. Kühn,³⁰ J. J. Lane,⁵⁵ J. S. Lange,³⁰ P. Larin,¹⁵ L. Lavezzi,^{63c} H. Leithoff,²⁸ M. Lellmann,²⁸ T. Lenz,²⁸ C. Li,³⁹ C. H. Li,³³ Cheng Li,^{60,48} D. M. Li,⁶⁸ F. Li,^{1,48} G. Li,¹ H. B. Li,^{1,52} H. J. Li,^{9,h} J. L. Li,⁴¹ J. Q. Li,⁴ Ke Li,¹ L. K. Li,¹ Lei Li,³ P. L. Li,^{60,48} P. R. Li,³² S. Y. Li,⁵⁰ W. D. Li,^{1,52} W. G. Li,¹ X. H. Li,^{60,48} X. L. Li,⁴¹ Z. B. Li,⁴⁹ Z. Y. Li,⁴⁹ H. Liang,^{60,48} H. Liang,^{1,52} Y. F. Liang,⁴⁵ Y. T. Liang,²⁵ L. Z. Liao,^{1,52} J. Libby,²¹ C. X. Lin,⁴⁹ B. Liu,^{42,g} B. J. Liu,¹ C. X. Liu,¹ D. Liu,^{60,48} D. Y. Liu,^{42,g} F. H. Liu,⁴⁴ Fang Liu,¹ Feng Liu,⁶ H. B. Liu,¹³ H. M. Liu,^{1,52} Huanhuan Liu,¹ Huihui Liu,¹⁷ J. B. Liu,^{60,48} J. Y. Liu,^{1,52} K. Liu,¹ K. Y. Liu,³⁴ Ke Liu,⁶ L. Liu,^{60,48} Q. Liu,⁵² S. B. Liu,^{60,48} Shuai Liu,⁴⁶ T. Liu,^{1,52} X. Liu,³² Y. B. Liu,³⁷ Z. A. Liu,^{1,48,52} Z. Q. Liu,⁴¹ Y. F. Long,^{38,k} X. C. Lou,^{1,48,52} F. X. Lu,¹⁶ H. J. Lu,¹⁸ J. D. Lu,^{1,52} J. G. Lu,^{1,48} X. L. Lu,¹ Y. Lu,¹ Y. P. Lu,^{1,48} C. L. Luo,³⁵ M. X. Luo,⁶⁷ P. W. Luo,⁴⁹ T. Luo,^{9,h} X. L. Luo,^{1,48} S. Lusso,^{63c} X. R. Lyu,⁵² F. C. Ma,³⁴ H. L. Ma,¹ L. L. Ma,⁴¹ M. M. Ma,^{1,52} Q. M. Ma,¹ R. Q. Ma,^{1,52} R. T. Ma,⁵² X. N. Ma,³⁷ X. X. Ma,^{1,52} X. Y. Ma,^{1,48} Y. M. Ma,⁴¹ F. E. Maas,¹⁵ M. Maggiora,^{63a,63c} S. Maldaner,²⁸ S. Malde,⁵⁸ Q. A. Malik,⁶² A. Mangoni,^{23b} Y. J. Mao,^{38,k} Z. P. Mao,¹ S. Marcello,^{63a,63c} Z. X. Meng,⁵⁴ J. G. Messchendorp,³¹ G. Mezzadri,^{24a} T. J. Min,³⁶ R. E. Mitchell,²² X. H. Mo,^{1,48,52} Y. J. Mo,⁶ N. Yu. Muchnoi,^{10,c} H. Muramatsu,⁵⁶ S. Nakhoul,^{11,f} Y. Nefedov,²⁹ F. Nerling,^{11,f} I. B. Nikolaev,^{10,c} Z. Ning,^{1,48} S. Nisar,^{8,i} S. L. Olsen,⁵² Q. Ouyang,^{1,48,52} S. Pacetti,^{23b} X. Pan,⁴⁶ Y. Pan,⁵⁵ A. Pathak,¹ P. Patteri,^{23a} M. Pelizaeus,⁴ H. P. Peng,^{60,48} K. Peters,^{11,f} J. Pettersson,⁶⁴ J. L. Ping,³⁵ R. G. Ping,^{1,52} A. Pitka,⁴ R. Poling,⁵⁶ V. Prasad,^{60,48} H. Qi,^{60,48} H. R. Qi,⁵⁰ M. Qi,³⁶ T. Y. Qi,² S. Qian,^{1,48} W.-B. Qian,⁵² Z. Qian,⁴⁹ C. F. Qiao,⁵² L. Q. Qin,¹² X. P. Qin,¹³ X. S. Qin,⁴ Z. H. Qin,^{1,48} J. F. Qiu,¹ S. Q. Qu,³⁷ K. H. Rashid,⁶² K. Ravindran,²¹ C. F. Redmer,²⁸ A. Rivetti,^{63c} V. Rodin,³¹ M. Rolo,^{63c} G. Rong,^{1,52} Ch. Rosner,¹⁵ M. Rump,⁵⁷ A. Sarantsev,^{29,d} Y. Schelhaas,²⁸ C. Schnier,⁴ K. Schoenning,⁶⁴ D. C. Shan,⁴⁶ W. Shan,¹⁹ X. Y. Shan,^{60,48} M. Shao,^{60,48} C. P. Shen,² P. X. Shen,³⁷ X. Y. Shen,^{1,52} H. C. Shi,^{60,48} R. S. Shi,^{1,52} X. Shi,^{1,48} X. D. Shi,^{60,48} J. J. Song,⁴¹ Q. Q. Song,^{60,48} W. M. Song,²⁷ Y. X. Song,^{38,k} S. Sosio,^{63a,63c} S. Spataro,^{63a,63c} F. F. Sui,⁴¹ G. X. Sun,¹ J. F. Sun,¹⁶ L. Sun,⁶⁵ S. S. Sun,^{1,52} T. Sun,^{1,52} W. Y. Sun,³⁵ Y. J. Sun,^{60,48} Y. K. Sun,^{60,48} Y. Z. Sun,¹ Z. T. Sun,¹ Y. H. Tan,⁶⁵ Y. X. Tan,^{60,48} C. J. Tang,⁴⁵ G. Y. Tang,¹ J. Tang,⁴⁹ V. Thoren,⁶⁴ B. Tsednee,²⁶ I. Uman,^{51d} B. Wang,¹ B. L. Wang,⁵² C. W. Wang,³⁶ D. Y. Wang,^{38,k} H. P. Wang,^{1,52} K. Wang,^{1,48} L. L. Wang,¹ M. Wang,⁴¹ M. Z. Wang,^{38,k} Meng Wang,^{1,52} W. H. Wang,⁶⁵ W. P. Wang,^{60,48} X. Wang,^{38,k} X. F. Wang,³² X. L. Wang,^{9,h} Y. Wang,⁴⁹ Y. Wang,^{60,48} Y. D. Wang,¹⁵ Y. F. Wang,^{1,48,52} Y. Q. Wang,¹ Z. Wang,^{1,48} Z. Y. Wang,¹ Ziyi Wang,⁵² Zongyuan Wang,^{1,52} D. H. Wei,¹² P. Weidenkaff,²⁸ F. Weidner,⁵⁷ S. P. Wen,¹ D. J. White,⁵⁵ U. Wiedner,⁴ G. Wilkinson,⁵⁸ M. Wolke,⁶⁴ L. Wollenberg,⁴ J. F. Wu,^{1,52} L. H. Wu,¹ L. J. Wu,^{1,52} X. Wu,^{9,h} Z. Wu,^{1,48} L. Xia,^{60,48} H. Xiao,^{9,h} S. Y. Xiao,¹ Y. J. Xiao,^{1,52} Z. J. Xiao,³⁵ X. H. Xie,^{38,k} Y. G. Xie,^{1,48} Y. H. Xie,⁶ T. Y. Xing,^{1,52} X. A. Xiong,^{1,52} G. F. Xu,¹ J. J. Xu,³⁶ Q. J. Xu,¹⁴ W. Xu,^{1,52} X. P. Xu,⁴⁶ L. Yan,^{9,h} L. Yan,^{63a,63c} W. B. Yan,^{60,48} W. C. Yan,⁶⁸ Xu Yan,⁴⁶ H. J. Yang,^{42,g} H. X. Yang,¹ L. Yang,⁶⁵ R. X. Yang,^{60,48} S. L. Yang,^{1,52} Y. H. Yang,³⁶

Y. X. Yang,¹² Yifan Yang,^{1,52} Zhi Yang,²⁵ M. Ye,^{1,48} M. H. Ye,⁷ J. H. Yin,¹ Z. Y. You,⁴⁹ B. X. Yu,^{1,48,52} C. X. Yu,³⁷ G. Yu,^{1,52} J. S. Yu,^{20,1} T. Yu,⁶¹ C. Z. Yuan,^{1,52} W. Yuan,^{63a,63c} X. Q. Yuan,^{38,k} Y. Yuan,¹ Z. Y. Yuan,⁴⁹ C. X. Yue,³³ A. Yuncu,^{51b,a} A. A. Zafar,⁶² Y. Zeng,^{20,1} B. X. Zhang,¹ Guangyi Zhang,¹⁶ H. H. Zhang,⁴⁹ H. Y. Zhang,^{1,48} J. L. Zhang,⁶⁶ J. Q. Zhang,⁴ J. W. Zhang,^{1,48,52} J. Y. Zhang,¹ J. Z. Zhang,^{1,52} Jianyu Zhang,^{1,52} Jiawei Zhang,^{1,52} L. Zhang,¹ Lei Zhang,³⁶ S. Zhang,⁴⁹ S. F. Zhang,³⁶ T. J. Zhang,^{42,g} X. Y. Zhang,⁴¹ Y. Zhang,⁵⁸ Y. H. Zhang,^{1,48} Y. T. Zhang,^{60,48} Yan Zhang,^{60,48} Yao Zhang,¹ Yi Zhang,^{9,h} Z. H. Zhang,⁶ Z. Y. Zhang,⁶⁵ G. Zhao,¹ J. Zhao,³³ J. Y. Zhao,^{1,52} J. Z. Zhao,^{1,48} Lei Zhao,^{60,48} Ling Zhao,¹ M. G. Zhao,³⁷ Q. Zhao,¹ S. J. Zhao,⁶⁸ Y. B. Zhao,^{1,48} Y. X. Zhao Zhao,²⁵ Z. G. Zhao,^{60,48} A. Zhemchugov,^{29,b} B. Zheng,⁶¹ J. P. Zheng,^{1,48} Y. Zheng,^{38,k} Y. H. Zheng,⁵² B. Zhong,³⁵ C. Zhong,⁶¹ L. P. Zhou,^{1,52} Q. Zhou,^{1,52} X. Zhou,⁶⁵ X. K. Zhou,⁵² X. R. Zhou,^{60,48} A. N. Zhu,^{1,52} J. Zhu,³⁷ K. Zhu,¹ K. J. Zhu,^{1,48,52} S. H. Zhu,⁵⁹ W. J. Zhu,³⁷ X. L. Zhu,⁵⁰ Y. C. Zhu,^{60,48} Z. A. Zhu,^{1,52} B. S. Zou,¹ and J. H. Zou¹

(BESIII Collaboration)

¹*Institute of High Energy Physics, Beijing 100049, People's Republic of China*

²*Beihang University, Beijing 100191, People's Republic of China*

³*Beijing Institute of Petrochemical Technology, Beijing 102617, People's Republic of China*

⁴*Bochum Ruhr-University, D-44780 Bochum, Germany*

⁵*Carnegie Mellon University, Pittsburgh, Pennsylvania 15213, USA*

⁶*Central China Normal University, Wuhan 430079, People's Republic of China*

⁷*China Center of Advanced Science and Technology, Beijing 100190, People's Republic of China*

⁸*COMSATS University Islamabad, Lahore Campus, Defence Road, Off Raiwind Road, 54000 Lahore, Pakistan*

⁹*Fudan University, Shanghai 200443, People's Republic of China*

¹⁰*G. I. Budker Institute of Nuclear Physics SB RAS (BINP), Novosibirsk 630090, Russia*

¹¹*GSI Helmholtzcentre for Heavy Ion Research GmbH, D-64291 Darmstadt, Germany*

¹²*Guangxi Normal University, Guilin 541004, People's Republic of China*

¹³*Guangxi University, Nanning 530004, People's Republic of China*

¹⁴*Hangzhou Normal University, Hangzhou 310036, People's Republic of China*

¹⁵*Helmholtz Institute Mainz, Johann-Joachim-Becher-Weg 45, D-55099 Mainz, Germany*

¹⁶*Henan Normal University, Xinxiang 453007, People's Republic of China*

¹⁷*Henan University of Science and Technology, Luoyang 471003, People's Republic of China*

¹⁸*Huangshan College, Huangshan 245000, People's Republic of China*

¹⁹*Hunan Normal University, Changsha 410081, People's Republic of China*

²⁰*Hunan University, Changsha 410082, People's Republic of China*

²¹*Indian Institute of Technology Madras, Chennai 600036, India*

²²*Indiana University, Bloomington, Indiana 47405, USA*

^{23a}*INFN Laboratori Nazionali di Frascati, I-00044 Frascati, Italy*

^{23b}*INFN and University of Perugia, I-06100 Perugia, Italy*

^{24a}*INFN Sezione di Ferrara, I-44122 Ferrara, Italy*

^{24b}*University of Ferrara, I-44122 Ferrara, Italy*

²⁵*Institute of Modern Physics, Lanzhou 730000, People's Republic of China*

²⁶*Institute of Physics and Technology, Peace Avenue 54B, Ulaanbaatar 13330, Mongolia*

²⁷*Jilin University, Changchun 130012, People's Republic of China*

²⁸*Johannes Gutenberg University of Mainz, Johann-Joachim-Becher-Weg 45, D-55099 Mainz, Germany*

²⁹*Joint Institute for Nuclear Research, 141980 Dubna, Moscow region, Russia*

³⁰*Justus-Liebig-Universitaet Giessen, II. Physikalisches Institut, Heinrich-Buff-Ring 16, D-35392 Giessen, Germany*

³¹*KVI-CART, University of Groningen, NL-9747 AA Groningen, Netherlands*

³²*Lanzhou University, Lanzhou 730000, People's Republic of China*

³³*Liaoning Normal University, Dalian 116029, People's Republic of China*

³⁴*Liaoning University, Shenyang 110036, People's Republic of China*

³⁵*Nanjing Normal University, Nanjing 210023, People's Republic of China*

³⁶*Nanjing University, Nanjing 210093, People's Republic of China*

³⁷*Nankai University, Tianjin 300071, People's Republic of China*

³⁸*Peking University, Beijing 100871, People's Republic of China*

³⁹*Qufu Normal University, Qufu 273165, People's Republic of China*


⁴⁰*Shandong Normal University, Jinan 250014, People's Republic of China*

⁴¹*Shandong University, Jinan 250100, People's Republic of China*

⁴²*Shanghai Jiao Tong University, Shanghai 200240, People's Republic of China*

⁴³*Shanxi Normal University, Linfen 041004, People's Republic of China*

- ⁴⁴Shanxi University, Taiyuan 030006, People's Republic of China
⁴⁵Sichuan University, Chengdu 610064, People's Republic of China
⁴⁶Soochow University, Suzhou 215006, People's Republic of China
⁴⁷Southeast University, Nanjing 211100, People's Republic of China
⁴⁸State Key Laboratory of Particle Detection and Electronics, Beijing 100049, Hefei 230026, People's Republic of China
⁴⁹Sun Yat-Sen University, Guangzhou 510275, People's Republic of China
⁵⁰Tsinghua University, Beijing 100084, People's Republic of China
^{51a}Ankara University, 06100 Tandogan, Ankara, Turkey
^{51b}Istanbul Bilgi University, 34060 Eyup, Istanbul, Turkey
^{51c}Uludag University, 16059 Bursa, Turkey
^{51d}Near East University, Nicosia, North Cyprus, Mersin 10, Turkey
⁵²University of Chinese Academy of Sciences, Beijing 100049, People's Republic of China
⁵³University of Hawaii, Honolulu, Hawaii 96822, USA
⁵⁴University of Jinan, Jinan 250022, People's Republic of China
⁵⁵University of Manchester, Oxford Road, Manchester M13 9PL, United Kingdom
⁵⁶University of Minnesota, Minneapolis, Minnesota 55455, USA
⁵⁷University of Muenster, Wilhelm-Klemm-Strasse 9, 48149 Muenster, Germany
⁵⁸University of Oxford, Keble Road, Oxford OX13RH, United Kingdom
⁵⁹University of Science and Technology Liaoning, Anshan 114051, People's Republic of China
⁶⁰University of Science and Technology of China, Hefei 230026, People's Republic of China
⁶¹University of South China, Hengyang 421001, People's Republic of China
⁶²University of the Punjab, Lahore-54590, Pakistan
^{63a}University of Turin, I-10125 Turin, Italy
^{63b}University of Eastern Piedmont, I-15121 Alessandria, Italy
^{63c}INFN, I-10125 Turin, Italy
⁶⁴Uppsala University, Box 516, SE-75120 Uppsala, Sweden
⁶⁵Wuhan University, Wuhan 430072, People's Republic of China
⁶⁶Xinyang Normal University, Xinyang 464000, People's Republic of China
⁶⁷Zhejiang University, Hangzhou 310027, People's Republic of China
⁶⁸Zhengzhou University, Zhengzhou 450001, People's Republic of China

 (Received 6 July 2020; revised 19 October 2020; accepted 27 January 2021; published 5 March 2021)

We present an analysis of the process $\psi(3686) \rightarrow \Omega^- \bar{\Omega}^+$ ($\Omega^- \rightarrow K^- \Lambda$, $\bar{\Omega}^+ \rightarrow K^+ \bar{\Lambda}$, $\Lambda \rightarrow p\pi^-$, $\bar{\Lambda} \rightarrow \bar{p}\pi^+$) based on a dataset of 448×10^6 $\psi(3686)$ decays collected with the BESIII detector at the BEPCII electron-positron collider. The helicity amplitudes for the process $\psi(3686) \rightarrow \Omega^- \bar{\Omega}^+$ and the decay parameters of the subsequent decay $\Omega^- \rightarrow K^- \Lambda$ ($\bar{\Omega}^+ \rightarrow K^+ \bar{\Lambda}$) are measured for the first time by a fit to the angular distribution of the complete decay chain, and the spin of the Ω^- is determined to be $3/2$ for the first time since its discovery more than 50 years ago.

DOI: [10.1103/PhysRevLett.126.092002](https://doi.org/10.1103/PhysRevLett.126.092002)

The discovery of the Ω^- [1] was a crucial step in our understanding of the microcosmos. It was a great triumph for the eightfold way model of baryons [2], and it led to the postulate of color charge [3]. A key feature of the eightfold way and the quark model is that the Ω^- spin is $J = 3/2$, a prediction that has never been unambiguously confirmed by experiment. The current best determination of $J = 3/2$ is based on an analysis [4] that assumes the spins of both the Ξ_c^0 and the Ω_c^0 are their quark model values of $J = 1/2$.

One of the conceptually simplest processes in which a baryon-antibaryon pair can be created is electron-positron annihilation. In this Letter, two Ω^- spin hypotheses, $J = 1/2$ or $J = 3/2$, are tested using the joint angular distribution of the sequential decays of the $e^+e^- \rightarrow \Omega^- \bar{\Omega}^+$ process. For the $J = 1/2$ hypothesis, two form factors are needed in the production of a baryon-antibaryon pair in electron-positron annihilation, and a clear vector polarization, strongly dependent on the baryon direction, is observed [5,6]. For the $J = 3/2$ hypothesis, the annihilation process involves four complex form factors [7]. In addition to vector polarization, the spin-3/2 fermions can have quadrupole and octupole polarization [8,9]. Polarization of the Ω^- can be studied using the chain of weak decays $\Omega^- \rightarrow K^- \Lambda$ and $\Lambda \rightarrow p\pi^-$, where the first decay is described by the ratio α_{Ω^-} and the relative phase

Published by the American Physical Society under the terms of the [Creative Commons Attribution 4.0 International license](https://creativecommons.org/licenses/by/4.0/). Further distribution of this work must maintain attribution to the author(s) and the published article's title, journal citation, and DOI. Funded by SCOAP³.

ϕ_{Ω^-} between the parity-conserving P -wave and parity-violating D -wave (S -wave for the $J = 1/2$ hypothesis) decay amplitudes. The decay parameters cannot be calculated reliably in theory [10–12], and only α_{Ω^-} has been previously measured [13–15].

The resonance production process $e^+e^- \rightarrow \psi(3686) \rightarrow \Omega^-\bar{\Omega}^+$ was observed by the CLEO-c experiment with 27 ± 5 and 326 ± 19 events using the double-tag and single-tag technique as described in Refs. [16] and [17], respectively. With the world's largest $\psi(3686)$ data sample of $(448.1 \pm 2.9) \times 10^6$ $\psi(3686)$ events accumulated in e^+e^- annihilation with the BESIII detector [18], we are able to select about 4000 $\psi(3686) \rightarrow \Omega^-\bar{\Omega}^+$ events, establish for the first time that the Ω^- spin is $J = 3/2$, and measure Ω^- polarizations in the $\psi(3686) \rightarrow \Omega^-\bar{\Omega}^+$ reaction and evidence for the dominance of the parity-violating D -wave amplitude in the weak decay $\Omega^- \rightarrow K^-\Lambda$.

For the $J = 3/2$ hypothesis, in helicity formalism [19,20], there are four helicity amplitudes in the production density matrix for $e^+e^- \rightarrow \psi(3686) \rightarrow \Omega^-\bar{\Omega}^+$ [21]. We define the ratios $A_{(1/2),(1/2)}/A_{(1/2),-(1/2)} = h_1 e^{i\phi_1}$, $A_{(3/2),(1/2)}/A_{(1/2),-(1/2)} = h_3 e^{i\phi_3}$, and $A_{(3/2),(3/2)}/A_{(1/2),-(1/2)} = h_4 e^{i\phi_4}$, where h_i and ϕ_i ($i = 1, 3, 4$) are real numbers to be determined from fits to data samples. The angular distribution is given by the trace of the Ω^- spin density matrix [21]: $1 + \alpha_{\psi(3686)} \cos^2 \theta_{\Omega^-}$, where $\alpha_{\psi(3686)} = [1 - 2(|h_1|^2 - |h_3|^2 + |h_4|^2)]/[1 + 2(|h_1|^2 + |h_3|^2 + |h_4|^2)]$. When considering the weak decays $\Omega^- \rightarrow K^-\Lambda$ and $\Lambda \rightarrow p\pi^-$, additional parameters α_{Ω^-} , α_{Λ} , and ϕ_{Ω^-} describing the ratio and relative phase between two helicity amplitudes are needed [21]. The joint angular distribution of θ_{Ω^-} , θ_{Λ} , ϕ_{Λ} , θ_p , and ϕ_p (see Fig. 1) is [21]

$$\rho_{3/2} = \sum_{\mu=0}^{15} \sum_{\nu=0}^3 r_{\mu} b_{\mu\nu} a_{\nu 0}. \quad (1)$$

For the $J = 1/2$ hypothesis, the joint angular distribution is defined as [21]

$$\rho_{1/2} = \sum_{\mu=0}^3 \sum_{\nu=0}^3 r_{\mu} a_{\mu\nu} a_{\nu 0}. \quad (2)$$

Here r_{μ} , $b_{\mu\nu}/a_{\mu\nu}$, and $a_{\nu 0}$ are defined in terms of the helicity amplitudes [21]. By fitting the joint angular distribution of the selected events with Eqs. (1) and (2), we can, in principle, obtain the helicity amplitudes and Ω^-/Λ decay parameters.

To maximize the reconstruction efficiency, a single-tag method is implemented in which only the Ω^- or the $\bar{\Omega}^+$ is reconstructed via $\Omega^- \rightarrow K^-\Lambda \rightarrow K^-p\pi^-$ or $\bar{\Omega}^+ \rightarrow K^+\bar{\Lambda} \rightarrow K^+\bar{p}\pi^+$, and the $\bar{\Omega}^+$ or Ω^- on the recoil side is inferred from the missing mass of the reconstructed particles. The following event selections are described for $\Omega^- \rightarrow K^-p\pi^-$ as an example; the same selections are also applied for the $\bar{\Omega}^+$ selection.

Charged tracks reconstructed from multilayer drift chamber (MDC) hits are required to be within a polar-angle (θ)

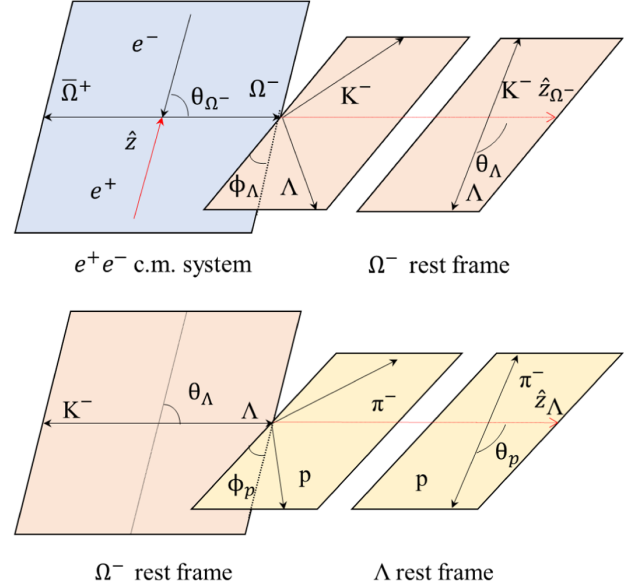


FIG. 1. Definition of the helicity angles used in the analysis. The helicity angles θ_{Ω^-} , θ_{Λ} , ϕ_{Λ} , θ_p , and ϕ_p are spherical coordinates of the Ω^- , Λ , and p momenta in three reference frames: the e^+e^- c.m. system and the Ω^- and Λ rest frames, respectively. The \hat{z} axis in the e^+e^- c.m. system points along the incoming positron, and \hat{z}_{Ω^-} is the Ω^- momentum direction. The polar axis direction in the Ω^- rest frame is \hat{z}_{Ω^-} , and \hat{y}_{Ω^-} is along $\hat{z} \times \hat{z}_{\Omega^-}$, where \hat{z}_{Λ} is the Λ momentum direction. The polar axis direction in the Λ rest frame is \hat{z}_{Λ} , and \hat{y}_{Λ} is along $\hat{z}_{\Omega^-} \times \hat{z}_{\Lambda}$.

range of $|\cos \theta| < 0.93$. To determine the species of final-state particles, specific energy loss (dE/dx) information is used to form particle identification (PID) probabilities for pion, kaon, and proton hypotheses. Charged particles are identified as the hypothesis with the highest probability, and only one K^- and one proton are required in each event. The rest of the negative charged tracks in an event are assumed to be π^- . To avoid potentially large differences between data and Monte Carlo (MC) simulation for very low momentum tracks, the transverse momenta of the p , K^- , and π^- tracks are required to be larger than 0.2, 0.1, and 0.05 GeV/ c , respectively.

The $\Lambda \rightarrow p\pi^-$ candidates are reconstructed by applying a vertex fit to the identified proton and a negatively charged pion with an invariant mass ($M_{p\pi^-}$) in the mass window of [1.110, 1.122] GeV/ c^2 . If more than one Λ candidate is found, the one with $p\pi^-$ invariant mass closest to the nominal Λ mass [22] is kept. The Λ candidate is then combined with a K^- track to reconstruct the Ω^- . A secondary vertex fit is applied to $K^-\Lambda$ to improve the Ω^- -mass resolution and to suppress backgrounds. The invariant mass of $K^-\Lambda$ ($M_{K^-\Lambda}$) is a requirement in the mass window of [1.663, 1.681] GeV/ c^2 . To obtain the antibaryon candidates $\bar{\Omega}^+$, we require the recoiling mass of $K^-\Lambda$ ($M_{K^-\Lambda}^{\text{recoil}}$) in the mass window of [1.640, 1.692] GeV/ c^2 . All the mass windows are determined by optimizing the

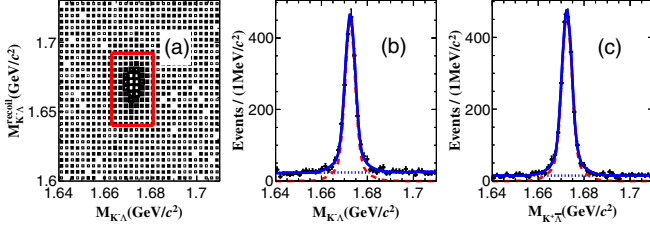


FIG. 2. (a) Distribution of $M_{K^-\Lambda}^{\text{recoil}}$ versus $M_{K^-\Lambda}$ of the selected $K^-\Lambda$ candidates in Ω^- reconstruction process. The red solid box shows the signal region of $\psi(3686) \rightarrow \Omega^-\bar{\Omega}^+$. (b) Projection onto $M_{K^-\Lambda}$ for events with $M_{K^-\Lambda}^{\text{recoil}}$ in the signal region. (c) The same as (b) but for $K^+\bar{\Lambda}$ tagged events. Dots with error bars are data, the solid blue curves show the results of the fit, the red dashed lines show the signal components of the fit, and the blue dotted lines show the background components of the fit.

figure of merit $s/\sqrt{s+b}$ with s being the number of signal events expected in data and b the number of the backgrounds in data estimated by using a normalization factor of sideband regions and the signal region.

The distribution of $M_{K^-\Lambda}$ versus $M_{K^-\Lambda}^{\text{recoil}}$ of the selected $K^-\Lambda$ candidates is shown in Fig. 2(a). A clear cluster of events in the data sample corresponding to $\psi(3686) \rightarrow \Omega^-\bar{\Omega}^+$ is observed in the signal region of the red box area.

An inclusive $\psi(3686)$ MC sample with 4×10^8 $\psi(3686)$ events is used to study the possible background sources [23] included in the simulation, and no peaking background is found. The continuum production of $\Omega^-\bar{\Omega}^+$ is expected to be very low and neglected. This is also checked with data collected at 3.65 GeV with an integrated luminosity of 49 pb^{-1} [about 7% of the $\psi(3686)$ data sample], and no significant $\Omega^-\bar{\Omega}^+$ signal is observed.

Events in the signal region, shown in Fig. 2(a), are used to perform the angular distribution analysis. After applying all the event selections, 2507 $\psi(3686) \rightarrow \Omega^-\bar{\Omega}^+$ candidates are selected by tagging the Ω^- (called the Ω^- sample) and 2238 candidates by tagging the $\bar{\Omega}^+$ (called the $\bar{\Omega}^+$ sample) by counting. The number of non- Ω^- background events is estimated from the numbers of events in the Ω^- -mass sideband as $M_{K^-\Lambda} \in [1.644, 1.653]$ or $[1.692, 1.701] \text{ GeV}/c^2$. The Ω^- ($\bar{\Omega}^+$) sample is estimated to contain 298 ± 17 (189 ± 14) background events.

An unbinned maximum-likelihood fit to the selected events is performed to measure the free parameters in the angular distribution. The likelihood function is defined as

$$\mathcal{L} = \prod_{j=1}^{N_t} W(\zeta_j|H) = \prod_{j=1}^{N_t} \frac{\rho(\zeta_j|H) \times \epsilon(\zeta_j)}{N(H)}, \quad (3)$$

where j is the candidate event number, $\rho(\zeta_j|H)$ is the angular distribution function for the cascade decay in Eqs. (1) and (2), $\zeta = \{\theta_\Omega, \theta_\Lambda, \phi_\Lambda, \theta_p, \phi_p\}$ are the angular distribution variables, and H contains the parameters to be determined from the fit. N_t is the number of the selected

TABLE I. Two sets of fit values of the helicity parameters in $\psi(3686) \rightarrow \Omega^-\bar{\Omega}^+$ decays of the spin-3/2 hypothesis. The first uncertainties are statistical, and the second ones systematic.

Parameter	Solution I	Solution II
h_1	$0.30 \pm 0.11 \pm 0.04$	$0.31 \pm 0.10 \pm 0.04$
ϕ_1	$0.69 \pm 0.41 \pm 0.13$	$2.38 \pm 0.37 \pm 0.13$
h_3	$0.26 \pm 0.05 \pm 0.02$	$0.27 \pm 0.05 \pm 0.01$
ϕ_3	$2.60 \pm 0.16 \pm 0.08$	$2.57 \pm 0.16 \pm 0.04$
h_4	$0.51 \pm 0.03 \pm 0.01$	$0.51 \pm 0.03 \pm 0.01$
ϕ_4	$0.34 \pm 0.80 \pm 0.31$	$1.37 \pm 0.68 \pm 0.16$
ϕ_Ω	$4.29 \pm 0.45 \pm 0.23$	$4.15 \pm 0.44 \pm 0.16$

events in the data samples. $N(H)$ is the normalization factor calculated with the MC integration method, and $\epsilon(\zeta_j)$ is the detection efficiency. Contributions from the background events to the likelihood have been considered by using events in the sideband regions of the Ω^- . The fit is performed by minimizing the objective function $S = -(\ln \mathcal{L}_{\text{data}} - \ln \mathcal{L}_{\text{bg}})$, where $\mathcal{L}_{\text{data}}$ is the likelihood function of events selected in the signal region of Ω^- and $\bar{\Omega}^+$ samples and \mathcal{L}_{bg} is the likelihood function of background events of these two single-tag samples estimated by the sideband method.

The decay parameters α_Λ and α_{Ω^-} are fixed to the Particle Data Group averages of previously measured values [5, 13–15]. Assuming that there is no CP violation in Ω^- and Λ decays, $\alpha_\Lambda = -\alpha_{\bar{\Lambda}} = 0.753 \pm 0.007$ and $\alpha_{\Omega^-} = -\alpha_{\bar{\Omega}^+} = 0.0154 \pm 0.0017$ [24]. A simultaneous fit is performed to the Ω^- and $\bar{\Omega}^+$ events selected from data in which the constraint $\phi_{\Omega^-} = -\phi_{\bar{\Omega}^+}$ is applied. The change of $2S$ of the fit assuming $J = 1/2$ and that of a linear combination of $J = 1/2$ and $J = 3/2$ is -232 with eight more free parameters, so we determine the significance of the $J = 3/2$ hypothesis over the $J = 1/2$ to be larger than 14σ and, thus, determine the spin of Ω^- as $3/2$ unambiguously. For the fit with $J = 3/2$, we find two solutions with identical fit quality, as shown in Table I. Tests with large MC sample confirm the existence of two solutions in such fits, although its origin is not obvious in the expression of the decay amplitude. The statistical and systematic covariance matrices for the two solutions are supplied in Supplemental Material [25].

The signal MC events generated according to phase space distribution are weighted with matrix elements calculated with the parameters obtained from the fits, and the weighted MC sample predictions are compared with data in five distributions of the helicity angle, with the background contributions estimated from the Ω^- sideband regions indicated as green histogram. We observe that the fit with Ω^- spin $J = 3/2$ describes data very well, while $J = 1/2$ fails to describe data, as shown in Fig. 3(a) for $\cos \theta_{\Lambda/\bar{\Lambda}}$, which has the most prominent difference. The moments M_6 and M_8 defined as $M_\mu = 1/N \sum_{j=0}^N \sum_{k=0}^3 b_{\mu,\kappa} a_{\kappa,0}$ are

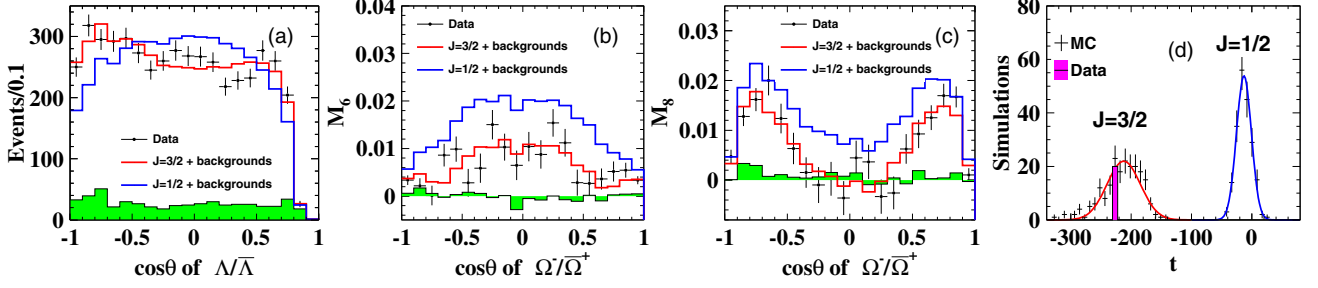


FIG. 3. (a) The $\cos\theta_{\Lambda/\bar{\Lambda}}$ distributions of data (dots with error bars) and fits with $J = 3/2$ (red histogram) and $J = 1/2$ (blue histogram) hypotheses; (b) and (c) are the M_6 and M_8 distributions of data and fit results; and (d) distribution of the test statistic $t = S^{J=1/2} - S^{J=3/2}$ for a series of MC simulations performed under the $J = 1/2$ (right peak) and $J = 3/2$ (left peak) hypotheses. The lines represent Gaussian fits to the simulated data points. The t value obtained from experimental data is indicated by the vertical bar.

compared between data and those two weighted MC samples, as shown in Figs. 3(b) and 3(c). Here N is the number of events in the data or MC samples. Clear preference of $J = 3/2$ over $J = 1/2$ is observed. Since the two sets of solutions describe the data equally well, we show the angular distributions for only one set of them.

The likelihood ratio $t = 2(S^{J=1/2} - S^{J=3/2})$ is used as a test variable to discriminate between the $J = 3/2$ and $J = 1/2$ hypotheses [28]. The MC sample for each hypothesis is generated according to its joint angular distribution, propagated through the detector model, and subjected to the same event selection criteria as the experimental data. Each MC subset has the same size as the real data samples and is assumed to have the same amount of background. The test statistic t distribution is shown in Fig. 3(d). The simulations for the right peak were performed under the $J = 1/2$ hypothesis, while those in the left peak correspond to the $J = 3/2$ hypothesis. It is clear that the t distributions of the two hypotheses are well separated. Since the t value from the data lies well within the left peak, our data favor the $J = 3/2$ hypothesis.

The following systematic uncertainties are considered for the angular distribution measurement. The tracking and PID efficiencies are studied with control samples of $J/\psi \rightarrow p\bar{p}\pi^+\pi^-$, $J/\psi \rightarrow \Lambda\bar{\Lambda}$ ($\Lambda \rightarrow p\pi^-$, $\bar{\Lambda} \rightarrow \bar{p}\pi^+$), $J/\psi \rightarrow K_S K^-\pi^+ + c.c.$, and $J/\psi \rightarrow pK^-\bar{\Lambda} + c.c.$, and the polar angle and transverse momentum (p_t) dependent efficiencies are measured. Subsequently, the efficiency of MC events is corrected by the two-dimensional efficiency scale factors and the uncertainty is estimated by varying the efficiency scale factors by one standard deviation for each p_t versus $\cos\theta$ bin. The differences between the new fit results and the nominal ones are taken as the systematic uncertainties. The uncertainty due to the background estimation is estimated by changing the Ω^- -sideband regions from [1.644, 1.653] and [1.692, 1.701] GeV/c^2 to [1.643, 1.653] and [1.692, 1.702] GeV/c^2 . The differences between fit results with and without changing sideband regions are taken as the systematic uncertainties. The uncertainties arising from the values of the fixed

parameters α_{Ω^-} and α_{Λ} are estimated by changing these two parameters by one standard deviation separately and then comparing the refitted parameters with the original results. We find that the uncertainty of α_{Ω^-} can be neglected. All of the above contributions are added in quadrature to obtain the total systematic uncertainties as shown in Table II.

From Table I, we find that the magnitudes of the amplitudes are about the same in the two solutions, while the phases ϕ_1 and ϕ_4 can be very different. All the h_i values are less than one, which means that the amplitude $A_{(1/2),-(1/2)}$ dominates the decay process. The value of ϕ_{Ω^-} provides information on whether the process is P -wave dominant ($\phi_{\Omega^-} = 0$) or D -wave dominant ($\phi_{\Omega^-} = \pi$). By comparing the maximum-likelihood values between the fit with ϕ_{Ω^-} fixed to zero or π and the nominal fit, we find that the significance for nonzero ϕ_{Ω^-} is 3.7σ and that for a non- $\pi\phi_{\Omega^-}$ is 1.5σ . Thus, ϕ_{Ω^-} favors the D -wave-dominant case, which differs from the theoretical predictions of P -wave dominance [29]. The ratio of D to P wave can be calculated as $|A_D|^2/|A_P|^2 = 2.4 \pm 2.0$ (solution I) and $|A_D|^2/|A_P|^2 = 3.3 \pm 2.9$ (solution II), where the uncertainty is the sum in quadrature of the statistical and systematic uncertainties. Allowing α_{Ω^-} to be determined by the fit, we obtain $\alpha_{\Omega^-} = -0.04 \pm 0.03$, which does not contradict the quoted result from previous experiments but with poorer precision [13–15].

TABLE II. Summary of the systematic uncertainties for the decay parameters in solution I (solution II) of $\psi(3686) \rightarrow \Omega^-\bar{\Omega}^+$.

	Track/PID	Background	α_{Λ}	Total
Δh_1	0.04 (0.04)	0 (0.01)	0 (0)	0.04 (0.04)
$\Delta\phi_1$	0.13 (0.12)	0.02 (0.04)	0.01 (0.01)	0.13 (0.13)
Δh_3	0.01 (0.01)	0 (0)	0.02 (0)	0.02 (0.01)
$\Delta\phi_3$	0.03 (0.03)	0.07 (0.02)	0 (0.01)	0.08 (0.04)
Δh_4	0.01 (0.01)	0 (0.01)	0 (0)	0.01 (0.01)
$\Delta\phi_4$	0.28 (0.11)	0.13 (0.12)	0.02 (0)	0.31 (0.16)
$\Delta\phi_{\Omega}$	0.16 (0.16)	0.17 (0.03)	0 (0.01)	0.23 (0.16)

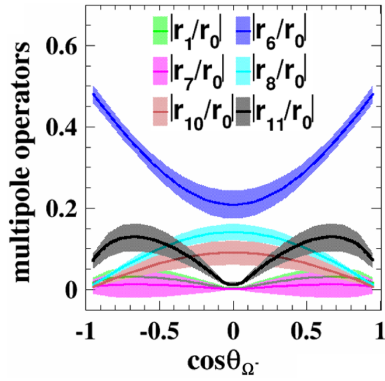


FIG. 4. The $\cos\theta_{\Omega^-}$ dependence of the multipolar polarization operators. The solid lines represent the central values, and the shaded areas represent \pm one standard deviation.

In conclusion, based on 448×10^6 $\psi(3686)$ events, we observe 4035 ± 76 $\psi(3686) \rightarrow \Omega^- \bar{\Omega}^+$ signal events. We conduct the first study of the angular distribution of the three-stage decay and found that the hypothesis of Ω^- with a spin of $3/2$ is preferred over a spin of $1/2$ with a significance of more than 14σ and establishes the spin of the Ω^- to be $3/2$ for the first time that is independent of any model-based assumptions. The helicity amplitudes of $\psi(3686) \rightarrow \Omega^- \bar{\Omega}^+$ and the decay parameter of $\Omega^- \rightarrow K^- \Lambda$, ϕ_{Ω^-} , are also measured for the first time. With the helicity amplitudes measured in Table I, $\alpha_{\psi(3686)} = 0.24 \pm 0.10$, where the uncertainty is the sum in quadrature of the statistical and systematic uncertainties.

With the helicity amplitudes measured in Table I, we calculate the $\cos\theta_{\Omega^-}$ dependence of the multipolar polarization operators as shown in Fig. 4. The uncertainties (statistical and systematic) are calculated using the covariance matrix of the fitted h_i and ϕ_i . For the process of $e^+e^- \rightarrow \psi(3686) \rightarrow \Omega^- \bar{\Omega}^+$, Ω^- particles not only have vector polarization (r_1), but also have quadrupole (r_6, r_7, r_8) and octupole (r_{10}, r_{11}) polarization contributions [8,9].

As a by-product, with the same data sample, the branching fraction for $\psi(3686) \rightarrow \Omega^- \bar{\Omega}^+$ is measured as $(5.85 \pm 0.12 \pm 0.25) \times 10^{-5}$, where the first uncertainty is statistical systematic and the second is systematic [25]. This result agrees with previous measurements [16,17] with improved precision.

The BESIII Collaboration thanks the staff of BEPCII and the IHEP computing center for their strong support. The authors thank Professor Zuotang Liang, Professor Yukun Song, Professor Xiaogang He, and Dr. Jusak Tandean for useful discussions. This work is supported in part by National Key Basic Research Program of China under Contract No. 2020YFA0406300; National Natural Science Foundation of China (NSFC) under Contracts No. 11625523, No. 11635010, No. 11735014, No. 11822506, No. 11835012, No. 11935015, No. 11935016, No. 11935018, and No. 11961141012;

the Chinese Academy of Sciences (CAS) Large-Scale Scientific Facility Program; Joint Large-Scale Scientific Facility Funds of the NSFC and CAS under Contracts No. U1732263 and No. U1832207; CAS Key Research Program of Frontier Sciences under Contracts No. QYZDJ-SSW-SLH003 and No. QYZDJ-SSW-SLH040; 100 Talents Program of CAS; Institute of Nuclear and Particle Physics (INPAC) and Shanghai Key Laboratory for Particle Physics and Cosmology; ERC under Contract No. 758462; German Research Foundation DFG under Contracts No. 443159800, Collaborative Research Center CRC 1044, FOR 2359, and GRK 214; Istituto Nazionale di Fisica Nucleare, Italy; Ministry of Development of Turkey under Contract No. DPT2006K-120470; National Science and Technology fund; Olle Engkvist Foundation under Contract No. 200-0605; STFC (United Kingdom); The Knut and Alice Wallenberg Foundation (Sweden) under Contract No. 2016.0157; The Royal Society, United Kingdom under Contracts No. DH140054 and No. DH160214; The Swedish Research Council; and U.S. Department of Energy under Contracts No. DE-FG02-05ER41374 and No. DE-SC-0012069.

^aAlso at Bogazici University, 34342 Istanbul, Turkey.

^bAlso at the Moscow Institute of Physics and Technology, Moscow 141700, Russia.

^cAlso at the Novosibirsk State University, Novosibirsk 630090, Russia.

^dAlso at the NRC ‘‘Kurchatov Institute,’’ PNPI, Gatchina 188300, Russia.

^eAlso at Istanbul Arel University, 34295 Istanbul, Turkey.

^fAlso at Goethe University Frankfurt, 60323 Frankfurt am Main, Germany.

^gAlso at Key Laboratory for Particle Physics, Astrophysics and Cosmology, Ministry of Education; Shanghai Key Laboratory for Particle Physics and Cosmology; Institute of Nuclear and Particle Physics, Shanghai 200240, People’s Republic of China.

^hAlso at Key Laboratory of Nuclear Physics and Ion-beam Application (MOE) and Institute of Modern Physics, Fudan University, Shanghai 200443, People’s Republic of China.

ⁱAlso at Harvard University, Department of Physics, Cambridge, Massachusetts 02138, USA.

^jPresent address: Institute of Physics and Technology, Peace Avenue 54B, Ulaanbaatar 13330, Mongolia.

^kAlso at State Key Laboratory of Nuclear Physics and Technology, Peking University, Beijing 100871, People’s Republic of China.

^lAlso at School of Physics and Electronics, Hunan University, Changsha 410082, China.

[1] V. E. Barnes *et al.*, *Phys. Rev. Lett.* **12**, 204 (1964).

[2] M. Gell-Mann, *Phys. Rev.* **125**, 1067 (1962).

[3] O. W. Greenberg, *Phys. Rev. Lett.* **13**, 598 (1964).

[4] B. Aubert *et al.* (BABAR Collaboration), *Phys. Rev. Lett.* **97**, 112001 (2006).

[5] M. Ablikim *et al.* (BESIII Collaboration), *Nat. Phys.* **15**, 631 (2019).

- [6] M. Ablikim *et al.* (BESIII Collaboration), *Phys. Rev. Lett.* **123**, 122003 (2019).
- [7] J. G. Korner and M. Kuroda, *Phys. Rev. D* **16**, 2165 (1977).
- [8] M. G. Doncel, L. Michel, and P. Minnaert, *Nucl. Phys.* **B38**, 477 (1972).
- [9] A. Z. Dubnickova, S. Dubnicka, and M. P. Rekaló, *Nuovo Cimento A* **109**, 241 (1996).
- [10] M. Suzuki, *Prog. Theor. Phys.* **32**, 138 (1964).
- [11] Y. Hara, *Phys. Rev.* **150**, 1175 (1966).
- [12] J. Finjord, *Phys. Lett. B* **76B**, 116 (1978).
- [13] Y. C. Chen, R. A. Burnstein, A. Chakravorty, A. Chan, W. S. Choong *et al.* (HyperCP Collaboration), *Phys. Rev. D* **71**, 051102(R) (2005).
- [14] L. C. Lu *et al.* (HyperCP Collaboration), *Phys. Lett. B* **617**, 11 (2005).
- [15] L. C. Lu, R. A. Burnstein, A. Chakravorty, Y. C. Chen, W. S. Choong *et al.* (HyperCP Collaboration), *Phys. Rev. Lett.* **96**, 242001 (2006).
- [16] S. Dobbs, A. Tomaradze, T. Xiao, K. K. Seth, and G. Bonvicini, *Phys. Lett. B* **739**, 90 (2014).
- [17] S. Dobbs, K. K. Seth, A. Tomaradze, T. Xiao, and G. Bonvicini, *Phys. Rev. D* **96**, 092004 (2017).
- [18] M. Ablikim *et al.* (BESIII Collaboration), *Nucl. Instrum. Methods Phys. Res., Sect. A* **614**, 345 (2010).
- [19] M. Jacob and G. C. Wick, *Ann. Phys. (N.Y.)* **7**, 404 (1959).
- [20] S. M. Berman and M. Jacob, Spin and parity analysis in two step decay processes, Stanford Linear Accelerator Center Technical Report No. SLAC-43, 1965.
- [21] E. Perotti, G. Fäldt, A. Kupsc, S. Leupold, and J. J. Song, *Phys. Rev. D* **99**, 056008 (2019).
- [22] M. Tanabashi *et al.* (Particle Data Group), *Phys. Rev. D* **98**, 030001 (2018).
- [23] X. Zhou, S. Du, G. Li, and C. Shen, *Comput. Phys. Commun.* **258**, 107540 (2021).
- [24] From the world average of $\alpha_{\Omega^-} \times \alpha_{\Lambda} = 0.0115 \pm 0.0013$ [13–15], by using the BESIII average of α_{Λ} and $\alpha_{\bar{\Lambda}}$ [5], $\alpha_{\Lambda} = 0.753 \pm 0.007$, we obtain $\alpha_{\Omega^-} = -\alpha_{\bar{\Omega}^+} = 0.0154 \pm 0.0017$. Here the uncertainties are combined statistical and systematic uncertainties, and CP symmetry is assumed in Λ and Ω decays.
- [25] See Supplemental Material at <http://link.aps.org/supplemental/10.1103/PhysRevLett.126.092002> for the statistical and systematic covariance matrices for the two solutions of the helicity amplitude fit, and for a brief description of the measurement of $\psi(3686) \rightarrow \Omega^- \bar{\Omega}^+$ branching fraction, which includes Refs. [26,27].
- [26] R. G. Ping, *Chin. Phys. C* **32**, 599 (2008).
- [27] M. Ablikim *et al.* (BESIII Collaboration), *Chin. Phys. C* **42**, 023001 (2018).
- [28] R. Aaij *et al.* (LHCb Collaboration), *Phys. Rev. D* **92**, 011102 (2015).
- [29] J. Tandean, *Phys. Rev. D* **70**, 076005 (2004).